Dependence of electric potentials at trench surfaces on ion angular distribution in plasma etching processes

2016 J. Phys. D: Appl. Phys. 49 105203

(http://iopscience.iop.org/0022-3727/49/10/105203)

IOP Publishing | Journal of Physics D: Applied Physics
J. Phys. D: Appl. Phys. **49** (2016) 105203 (10pp) | doi:10.1088/0022-3727/49/10/105203

Dependence of electric potentials at trench surfaces on ion angular distribution in plasma etching processes

A P Palov[1], Yu A Mankelevich[1], T V Rakhimova[1] and M R Baklanov[2]

[1] Skobeltsyn Institute of Nuclear Physics, Lomonosov Moscow State University, Moscow 119991, Russian Federation
[2] IMEC, Heverlee 3001, Belgium

E-mail: a.palov@mics.msu.su

Received 11 September 2015, revised 8 December 2015
Accepted for publication 18 December 2015
Published 8 February 2016

Abstract
Ion-stimulated etching of dielectrics in radio frequency plasma results in positive charging of a trench bottom because of the significant difference in the angular distribution functions of ions and electrons. They are anisotropic for ions and quasi-isotropic for electrons. The charging leads to a decrease in the energy of the ions bombarding the trench bottom and to undesirable sputtering of the walls near the trench bottom because of the curving of the ion trajectories. This process is normally investigated by Monte Carlo methods in the absence of experimental data. In this paper the analytical dependence of the ion flux bombarding the trench bottom on a trench aspect ratio and ion angular distribution function is obtained. Numerical calculations of the electric potential on the trench bottom for a set of trench aspect ratios and angles of the ion angular distribution function were performed based on a Monte Carlo method to demonstrate the ion flux and electric potential correlated well with each other. The proposed formula for an ion flux is suggested to be helpful for analyzing charging the trenches with different aspect ratios in plasma with an arbitrary angular ion distribution function.

Keywords: plasma etching, trench charging, aspect ratio, ion angular distribution function

(Some figures may appear in colour only in the online journal)

I. Introduction

High-precision etching of narrow trenches is a key issue in the advanced fabrication of microelectronic devices [1]. The etching of insulating materials is accompanied by a charging effect whose physical origin is due to the differences in the electron and ion angular distributions. The charging effect induces many serious damage problems in plasma processing such as bowing, trenching, etching rate reduction, and even the breakdown of lower level device elements [2–5]. The reduction in device sizes and multilayer structures requires a high-aspect ratio in SiO_2 etching and in the etching of new dielectric materials with a low dielectric constant [6]. As a result, the charging effect becomes even more important. Thus, understanding the effects of surface charging is key to the accurate description of etching at the nanometer scale.

Numerical simulation is the main tool to describe plasma etching of dielectrics and semiconductors in present-day complementary metal–oxide–semiconductor (CMOS) technology. The simulation procedure is normally split into two parts, such as discharge modeling and plasma–surface interaction [7, 8]. The last one includes the simulation of ion-stimulated processes on the surface of a dielectric or semiconductor [9, 10]. As was mentioned above, the plasma–insulator surface interaction leads to charging of the insulator trenches in addition to etching. The direct measurement of the electric potential inside trenches has been a complex problem until now, so since the beginning of the 1990s the main way to describe the charging process has been the numerical modeling of electron and ion trajectories [11–18].

Until recently [19–21] it has mostly been suggested that the angular dispersion of ionic velocities around the direction to the normal to the film surface is not more than ~5° in the plasma sheath of a radio frequency-biased substrate. As a sequence all the trench etching and charging calculations were carried out based on Monte Carlo methods for this ion angular distribution function (IADF). Nevertheless, some experiments showed the angular dispersions can exceed ~5° [22, 23] for low-pressure plasma, and the question as to what happens for larger angles is thus still open.

In this paper, we applied the Monte Carlo approach to calculate the electric potential on the trench bottom for angular dispersions larger than ~5°. Suggesting the electric potential and an ion flux on the trench bottom may correlate, we found and presented the analytical dependences of the ion flux on the trench bottom on aspect ratios (ARs) and the IADF, to the best of our knowledge, for the first time. We also show further that the ion flux and electric potential dependences on different trench ARs and IADFs match each other nicely.

The worth of the obtained analytical expression for the ion flux and its correlation with the numerically calculated electric potential on the ARs and the IADF is twofold. First, it can be used for a quick analytic estimation of the electric potential on the trench bottom without the necessity of running time-consuming Monte Carlo charging programs. Second, it can easily be included in Monte Carlo etching codes to consider the electric field impact on the ionic and electron trajectories in a trench.

The formulation of the problem and the basic idea of our analytical approach to obtain the ion flux on the trench bottom will be described in section II. A detailed discussion of the obtained analytical results for trenches with ARs of 1–6 and trench widths of 12 nm for 45–180 eV ion flux and their validation by Monte Carlo calculations will be presented in section III. Finally, we give our conclusion in section IV.

II. Theory

The electric potential on the trench bottom in comparison with the one on the trench entrance depends on the net charge left by the ions and electrons on the trench bottom. The number of ions coming to the trench bottom is defined by their flux from the plasma, while the number of electrons coming to the trench bottom is governed by their flux from the plasma and by the flux generated as a result of the secondary electron emission (SEE) from the trench walls. The numerous Monte Carlo calculations have shown that the electric potentials in the trenches do not depend on their width and height, but only depend on their ARs [24, 25].

To the best of our knowledge the dependence of the electric potential in a trench on the IADF in plasma has not been investigated. In this paper we present an approach that gives analytically a qualitative dependence of the potential on the trench bottom on the trench ARs and the IADF. This approach is based on the suggestion that this dependence is basically defined by an ion flux on the trench bottom. The argument for this hypothesis is that the obtained analytic dependences are well correlated to the numerical results obtained by Monte Carlo calculations. Unfortunately, at the moment the direct measurements of the electric potential inside dielectric trenches do not exist to validate our results.

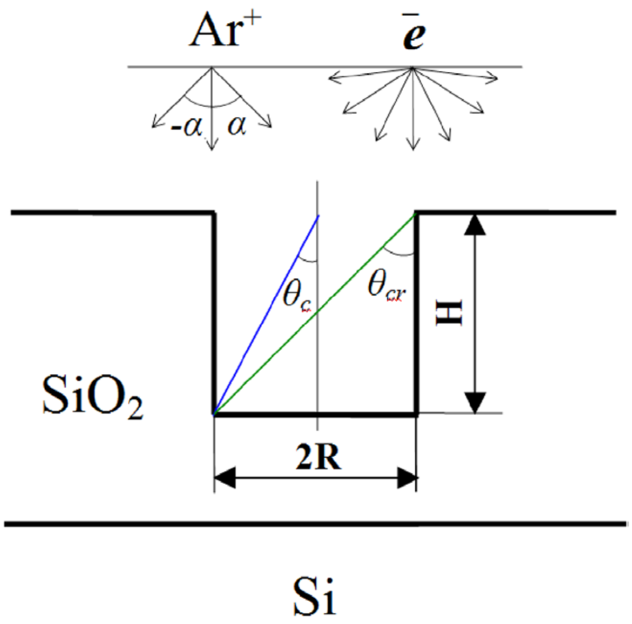

Figure 1. Geometry of the periodic trenches, critical angles, and the angular distributions of the ions and electrons.

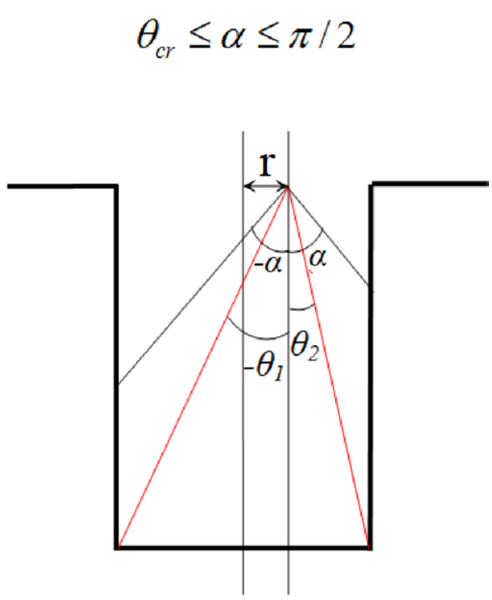

Figure 2. Integration limits for calculations of the net ion flux on the trench bottom for maximal polar angles in the range of $\theta_{cr} \leqslant \alpha \leqslant \pi/2$.

The next stage of development of the presented model is to consider the generation of the secondary electrons as a result of the SEE from the trench walls. This should lead to the opportunity of calculating the absolute value of the electric potential in a trench, and not only its qualitative behavior. We plan to complete it in our next publication.

Thus, let us define the ion flux f_{ion} in two-dimensional (2D) space as the number of ions bombarding a unit of a trench length per a unit of time. Let us assume that monoenergetic ion fluxes have a simplified shape of the ion angular distribution f_{ion}, namely, a constant in the range of $0 < \theta < \alpha$ and zero otherwise, where a polar angle θ is defined as the angle from a direction to the normal to the film and α is its maximal value,

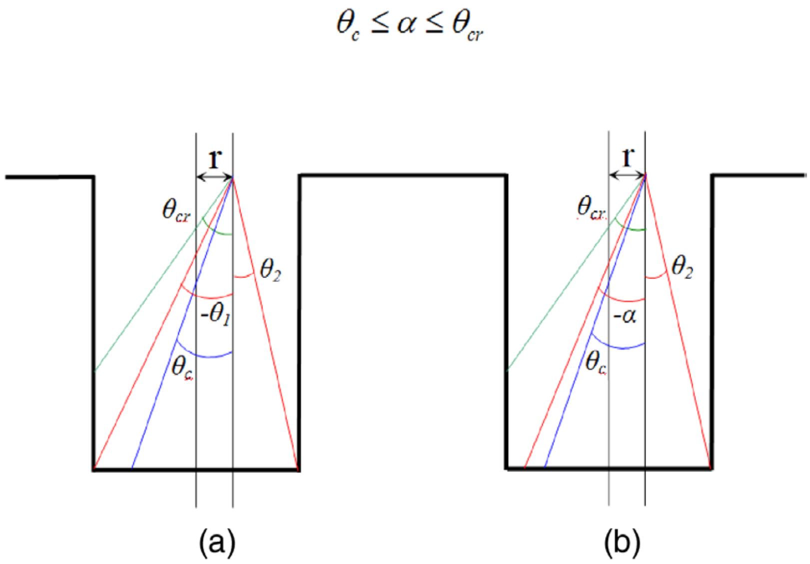

Figure 3. (a)–(b) Integration limits for calculations of the net ion flux on the trench bottom for maximal polar angles in the range of $\theta_c \leqslant \alpha \leqslant \theta_{cr}$ for cases $\alpha > \theta_1$ (a) and $\alpha < \theta_1$ (b).

see figure 1. As is known from plasma processing technology, the IADF is anisotropic, i.e. $\alpha < \pi/2$, in comparison with an electron one, which is approximately isotropic, i.e. $\alpha = \pi/2$, in most cases. To normalize f_{ion} on the net flux N_{ion} coming into the trench we need to integrate it over all the ion angles and positions r at the trench entrance, see figure 1:

$$N_{ion} = \int_{-R}^{R} dr \int_{-\alpha}^{\alpha} f_{ion} \cos\theta \, d\theta \tag{1}$$

then the f_{ion} constant is given by:

$$f_{ion} = \frac{N_{ion}}{4R\sin\alpha}. \tag{2}$$

We will calculate the ion flux on the trench bottom assuming the ion trajectories are straight lines. Note this assumption is reasonable if the ion energies exceed considerably the typical values of a negative potential near the trench entrance of a few eV and a positive potential on the trench bottom of a few tens eV. For convenience of calculation one needs to introduce a value of a critical angle $\Theta_{cr} = \tan^{-1}(1/A)$, see figure 1, where $A = H/2R$ is an AR of the trench with its width of $2R$ and its height of H.

Thus, the net ion flux on the trench bottom equals, see figures 2–4:

$$F_{ion}(\alpha, A) = 2\int_{0}^{R} dr \int_{-\theta_1}^{\theta_2} f_{ion} \cos\theta \, d\theta \tag{3}$$

where factor 2 appears because of the task symmetry relative to the trench axis. To integrate equation (3) we need to consider three distinctive cases.

In the first case, when the maximal angle α belongs to a range:

$$\theta_{cr} \leqslant \alpha \leqslant \pi/2 \tag{4}$$

one needs use the following integration limits, see figure 2, in red:

$$\theta_1 = \tan^{-1}\frac{R+r}{H}$$
$$\theta_2 = \tan^{-1}\frac{R-r}{H} \tag{5}$$

because the ions coming into the trench from any r position are always able to reach any position on the trench bottom. Then, integrating equation (3) over the limits given by equation (5) and substituting the value of f_{ion} from equation (2) into equation (3) one directly obtains:

$$F_{ion}(\alpha, A) = \frac{N_{ion}}{\sin\alpha}\left\{\sqrt{1+A^2} - A\right\} \tag{6}$$

The details of these calculations are presented in the appendix in equations (A.1) and (A.2) at the end of the paper.

In the second case the angular range is:

$$\theta_c \leqslant \alpha \leqslant \theta_{cr} \tag{7}$$

and one needs use the following limits of integration to calculate $F_{ion}(\alpha, A)$, see figures 3(a) and (b):

$$\theta_1 = \begin{cases} \alpha, & r > r^* \\ \tan^{-1}\dfrac{R+r}{H}, & r < r^* \end{cases}$$
$$\theta_2 = \tan^{-1}\frac{R-r}{H} \tag{8}$$

where $r^* = H \times \tan(\alpha) - R$. Figures 3(a) and (b) demonstrate the angle θ_2 is always the same because α is always less than θ_2. As we can see from figures 3(a) and (b), if the value $\theta_1 = \tan^{-1}\{(R+r)/H\}$ is less than α, see figure 3(a), we need to use it and $\theta_1 = \alpha$ in the opposite case, see figure 3(b). The parameter r^* is defined from the equality $\alpha = \tan^{-1}\{(R+r^*)/H\}$.

Substituting the value of f_{ion} from equation (2) in equation (3) and its integration with the limits of equation (8) leads to:

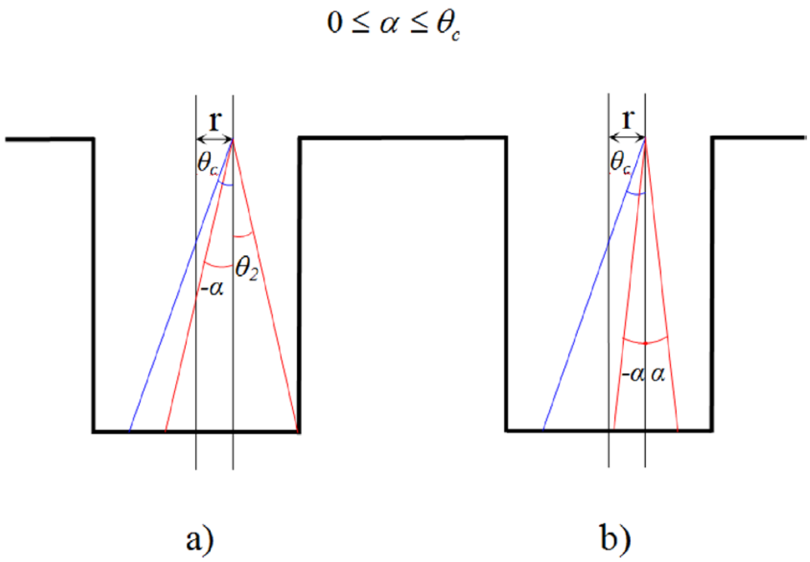

Figure 4. (a)–(b) Integration limits for calculations of the net ion flux on the trench bottom for maximal polar angles in the range of $0 \leqslant \alpha \leqslant \theta_c$ for cases $\alpha > \theta_2$ (a) and $\alpha < \theta_2$ (b).

$$F_{\text{ion}}(\alpha, A) = N_{\text{ion}}\left\{1 - A \times \frac{1-\cos\alpha}{\sin\alpha}\right\} \tag{9}$$

The details of these calculations are given in the appendix in equations (A.3)–(A.5) at the end of the paper.

In the third (last) case, when the ion angular distribution belongs to the angular interval:

$$0 \leqslant \alpha \leqslant \theta_c \tag{10}$$

the following integration limits must be used, see figures 4(a) and (b):

$$\begin{aligned} &\theta_1 = \alpha \\ &\theta_2 = \begin{cases} \alpha, & r \leqslant r^* \\ \tan^{-1}\dfrac{R-r}{H}, & r \geqslant r^* \end{cases} \end{aligned} \tag{11}$$

where $r^* = R - H \times \tan(\alpha)$. As we can see from figures 4(a) and (b) the angle θ_1 equals α because it is always less than θ_c, while the angle θ_2 is a minimal one between α, see figure 4(b), and $\tan^{-1}\{(R-r)/H\}$, see figure 4(a), and the parameter r^* is extracted from their equality. It is interesting to note in the last case that we obtain the same result for $F_{\text{ion}}(\alpha, A)$ after the integration of equation (3) with the limits of equation (11) as the one in equation (9). The details are given in the appendix in equations (A.6)–(A.8) at the end of the paper.

In the case of $\alpha = 0$ the ion angular distribution is presented by delta-function directed to the surface normal, and the use of equation (9) leads to $F_{\text{ion}}(\alpha, A) = N_{\text{ion}}$, i.e. all ions coming into the trench reach its bottom, as must be the case.

Combining the second, equation (6), and the third, equation (9), cases the total result for $F_{\text{ion}}(\alpha, A)$ can be written as:

$$F_{\text{ion}}(\alpha, A) = \begin{cases} N_{\text{ion}}\left\{1 - A \times \dfrac{1-\cos\alpha}{\sin\alpha}\right\}, & 0 \leqslant \alpha \leqslant \theta_{\text{cr}} \\ \dfrac{N_{\text{ion}}}{\sin\alpha}\left\{\sqrt{1+A^2} - A\right\}, & \theta_{\text{cr}} \leqslant \alpha \leqslant \pi/2 \end{cases} \tag{12}$$

Thus, equation (12) gives the explicit analytic dependence of the total ion flux on the trench bottom on the trench AR and ion angular distribution, which is the main result of our paper.

It is rather useful to analyze the distribution of the ion fluxes over the trench walls and bottom to understand qualitatively how different sectors of the trench surface may be charged up.

Let us re-write equation (3) to calculate the ion flux on the left wall for the initial flux position of the trench inlet, see figure 5(a), for convenience as:

$$F_{\text{ion}}(\alpha, A) = f_{\text{ion}} \int_0^{r^*} \mathrm{d}r \int_{-\alpha}^{-\theta_2} \cos\theta\, \mathrm{d}\theta \tag{13}$$

where $\theta_2 = \tan^{-1}(r/H)$ and the integration over r is made from 0 to $r^* = H \times \tan(\alpha)$ for $0 \leqslant \alpha \leqslant \theta_{\text{cr}}$, and up to $r^* = 2R$ for $\theta_{\text{cr}} \leqslant \alpha \leqslant \pi/2$. Then we can introduce a grid on the left wall, see figure 5(b), and define $H_i = i \times h$ and $H_{i+1} = (i+1) \times h$, where h is a grid spacing in the trench height direction, and then the ion flux on the ith cell of the grid $\Delta F_i = F_{\text{ion},\, i+1}(\alpha, A_{i+1}) - F_{\text{ion},\, i}(\alpha, A_i)$ with $A_i = H_i/2R$ can be written:

$$\Delta F_i(\alpha) = \begin{cases} \dfrac{N_{\text{ion}}}{2}\dfrac{h}{2R}\dfrac{1-\cos\alpha}{\sin\alpha}, & 0 \leqslant \alpha \leqslant \theta_{\text{cr}} \\ \dfrac{N_{\text{ion}}}{2\sin\alpha}\left\{\dfrac{h}{2R} + \sqrt{1+\left[\dfrac{ih}{2R}\right]^2} - \sqrt{1+\left[\dfrac{(i+1)h}{2R}\right]^2}\right\}, & \theta_{\text{cr}} \leqslant \alpha \leqslant \dfrac{\pi}{2} \end{cases} \tag{14}$$

The details of these calculations are shown in the appendix in equations (A.9)–(A.12) at the end of the paper.

In order to describe the ion flux on the jth cell of the trench bottom we present the cell length as $\Delta r = 2R/(L-1)$, where L is a number of grid nodes, and re-write equation(3):

$$\Delta F_j = \frac{N_{\text{ion}}}{2\sin\alpha} \int_{r_{\min}}^{r_{\max}} \mathrm{d}r \int_{-\theta_1}^{-\theta_2} \cos\theta\, \mathrm{d}\theta \tag{15}$$

where $r_{\max} = \min(1,\ j \times \Delta r/2R + A \times \tan(\alpha))$ and $r_{\min} = \max(0,\ (j+1) \times \Delta r/2R - A \times \tan(\alpha))$, while the angular integration limits are:

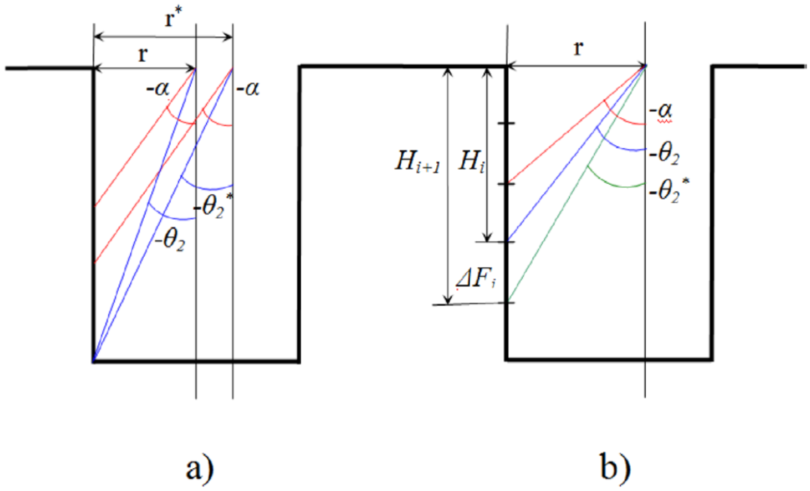

Figure 5. Integration limits for calculations of the net ion flux on the trench wall from two positions on the trench inlet (a) and the ion flux ΔFi on the ith cell of the trench wall for an arbitrary point on the trench inlet (b).

$$\theta_2 = \tan^{-1}\left[\frac{r - j \times \Delta r/2R}{H/2R}\right]$$
$$\theta_1 = \tan^{-1}\left[\frac{r - (j-1) \times \Delta r/2R}{H/2R}\right] \quad (16)$$

Here r is normalized by $2R$. Substituting the limits given by equation (16) in equation (15) one may show, see equations (A.13) and (A.14) in the appendix, the ion flux on the jth cell of the trench bottom is:

$$\Delta F_j = \frac{N_{\text{ion}}}{2\sin\alpha}\left\{\sqrt{A^2 + (r_{\min} - r_j)^2} - \sqrt{A^2 + (r_{\max} - r_j)^2} + \sqrt{A^2 + (r_{\max} - r_{j-1})^2} - \sqrt{A^2 + (r_{\min} - r_{j-1})^2}\right\} \quad (17)$$

where $r_{j-1} = (j-1)\Delta r/2R$ and $r_j = j\Delta r/2R$. For electrons similar formulas to equations(1)–(17) can be obtained by the substitution $\alpha = \pi/2$. However, they must be applied only as initial conditions for unsteady calculations of the trench charging because the electron trajectories for the typical discharge energies of ~3 eV are too sensitive to the typical potential of a few eV at the trench entrance and a few tens eV [24] on the trench bottom. The ion trajectories are also sensitive to the electric potential, but their energies noticeably exceed the negative potential at the trench entrance and the positive potential on the trench bottom. Thus, the obtained formulas given by equations (12), (14) and (17) can be applied to estimate the potential on the trench bottom.

III. Results and discussion

First of all we consider how the ion fluxes are distributed over the trench surface including the walls and the bottom. Figure 6 demonstrates the ion flux distribution over the trench height of 0 to 8 ARs computed using equation (14). It can be seen that all the curves have straight-line segments until the heights calculated from the equality of $\alpha = 2\theta_c$. The ion flux on the trench height cells for the chosen angle α is a constant during this segment, and the wall is charging uniformly positive over the height. The red line shows the ion flux distribution over the trench height for fully isotropic ion angular distribution. Note, the electron flux over the trench height will be the same if we neglect the negative potential on the trench entrance and the positive one on the trench bottom, i.e. in the case of the beginning of the trench charging when these potentials are to small to affect the electron trajectories. Figure 6 shows in red the electron fluxes on the wall cells near the trench inlet are the largest, and thus this part of the trench wall will become negatively charged. This fact is confirmed by numerous Monte Carlo calculations [24].

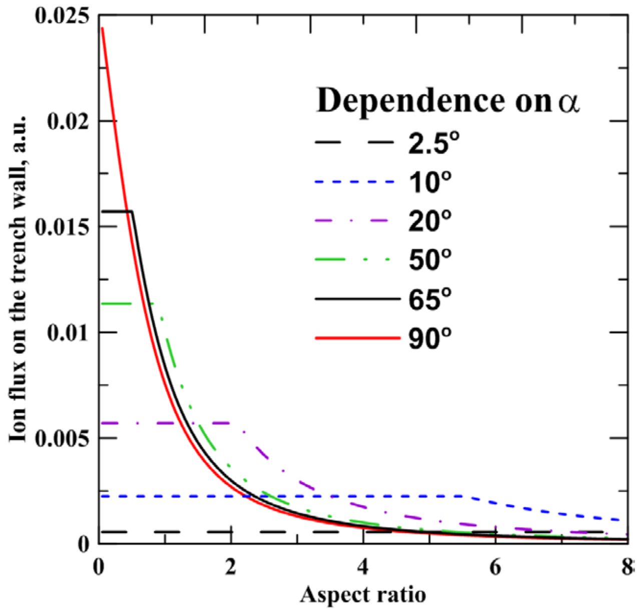

Figure 6. Distribution of the ion flux on the trench wall as a function of the aspect ratios.

Figures 7(a) and (b) present the ion flux distribution over the trench bottom calculated using equation (16) for the maximal angles of $\alpha = 2.5°$ and $7.5°$, consequently. In both cases

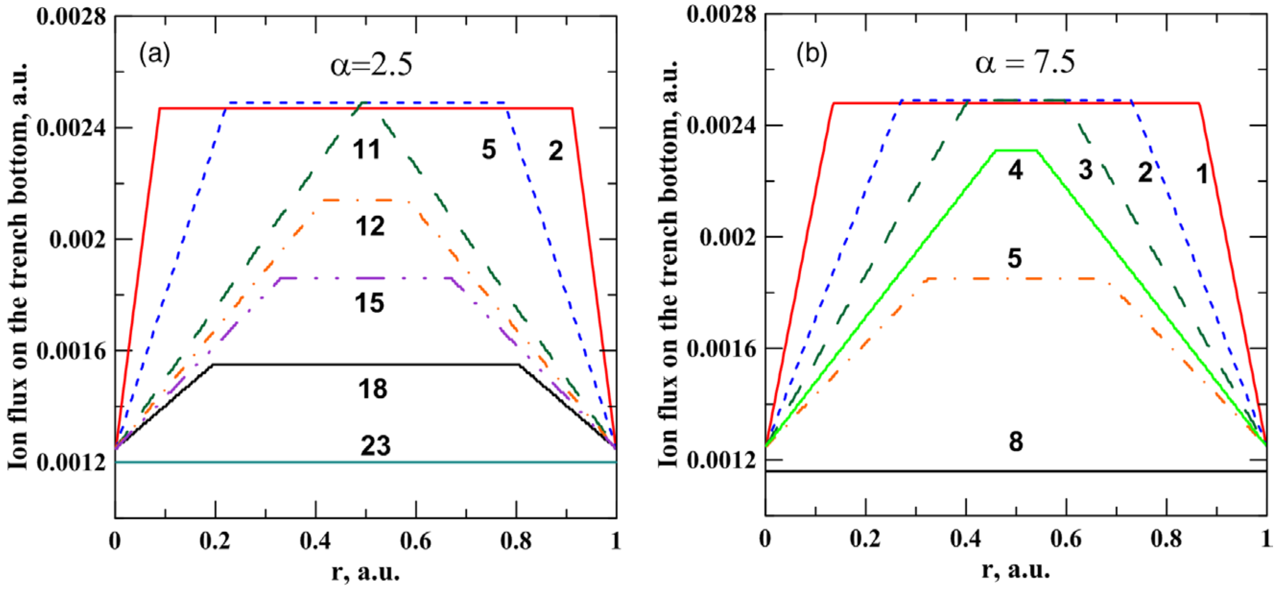

Figure 7. (a) The ion flux on the trench bottom as a function of its position $r_j = j\Delta r/2R$ on the trench bottom, see equation (17), for the maximal polar angle of 2.5° and aspect ratios $A = 2$, 5, 11, 12, 15, 18, and 23. (b) The ion flux on the trench bottom as a function of its position $r_j = j\Delta r/2R$ on the trench bottom, see equation (17), for the maximal polar angle of 7.5° and aspect ratios $A = 1$, 2, 3, 4, 5, and 8.

the ion fluxes have long flat central parts, especially for small ARs such as $A = 1$–2. A further increase in the AR leads to focusing the magnitude of the ion fluxes on the center of the trench bottom. We can also see from figures 7(a) and (b) that for the ARs larger than $A = 1/\tan(\alpha)$, ~22.904 at $\alpha = 2.5°$ and ~7.596 at $\alpha = 7.5°$, the magnitude of the ion fluxes drops rapidly and its distribution over the trench bottom becomes almost uniform. This means the ions starting from any point of the trench inlet are able to reach any point on the trench bottom and the total fluxes on any cell of the trench bottom become the same. It can be seen from equation (15) that the integration limits over the initial positions of ions on the trench inlet are equal to $r_{\min} = 0$ and $r_{\max} = 1$ and do not depend on the position of the jth cell on the trench bottom. The values of the ion fluxes will decrease with an increase in the trench depth (H) because the integration limits over the angles will make the integral smaller in accordance with equation (16), i.e. the input in the total ion flux on the trench bottom cell from any point of the trench inlet becomes smaller.

Figures 7(a) and (b) also show the interesting behavior of the ion fluxes for $A < 1/\tan(\alpha)$, when they, having flat central parts, shrink to the point at $A = 1/\{2\tan(\alpha)\}$ in accordance with equation (15), i.e. $A = 3.798$ at $\alpha = 7.5°$ and $A = 11.452$ at $\alpha = 2.5°$. Note this happens when the flux on the central cell of the trench bottom is the first one, which is the sum of the ion fluxes from all points of the trench inlet.

Let us suggest the number of positive charges on the sectors of the trench bottom is directly proportional to the ion flux in this sector. A surplus of the positive charge in the center of the trench bottom leads to the appearance of the radial electric field curving ion trajectories towards the trench walls near its bottom. This fact was confirmed by numerous Monte Carlo calculations by different authors. From figures 7(a) and (b) one can see the large potential gradients at both edges of the trench bottom towards the wall for all $A < 1/\tan(\alpha)$.

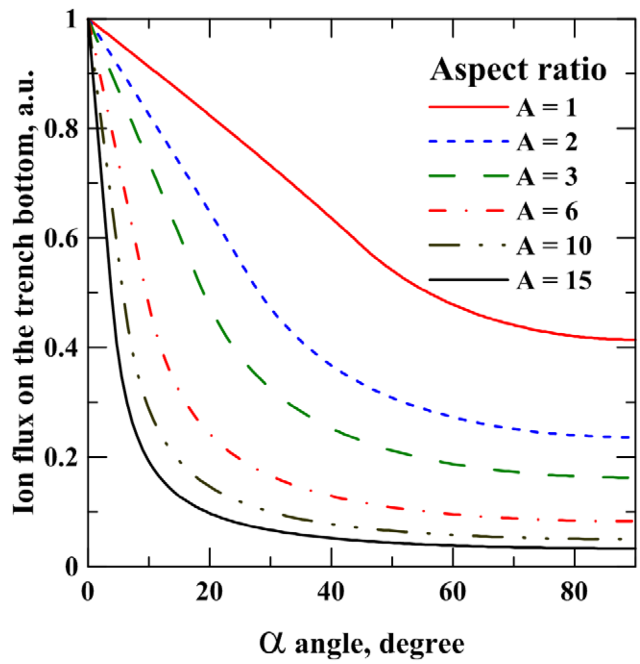

Figure 8. The net ion flux on the trench bottom as a function of the maximal polar angle α of the ion angular distribution function for different aspect ratios.

The net ion flux on the trench bottom as a function of the maximal angle $\boldsymbol{\alpha}$ for different trench ARs is calculated on the base of equation (12) and is presented in figure 8. It can be seen that the general form of this dependence is described by a monotonous function falling off towards the area of large angles. All the curves approach some constant limits at the angle $\alpha = \pi/2$ corresponding to the isotropic angular distribution of ions. One can see from figure 8 that the increase in the AR leads to a sharp decrease in the net ion flux on the trench bottom in the area of small values of α.

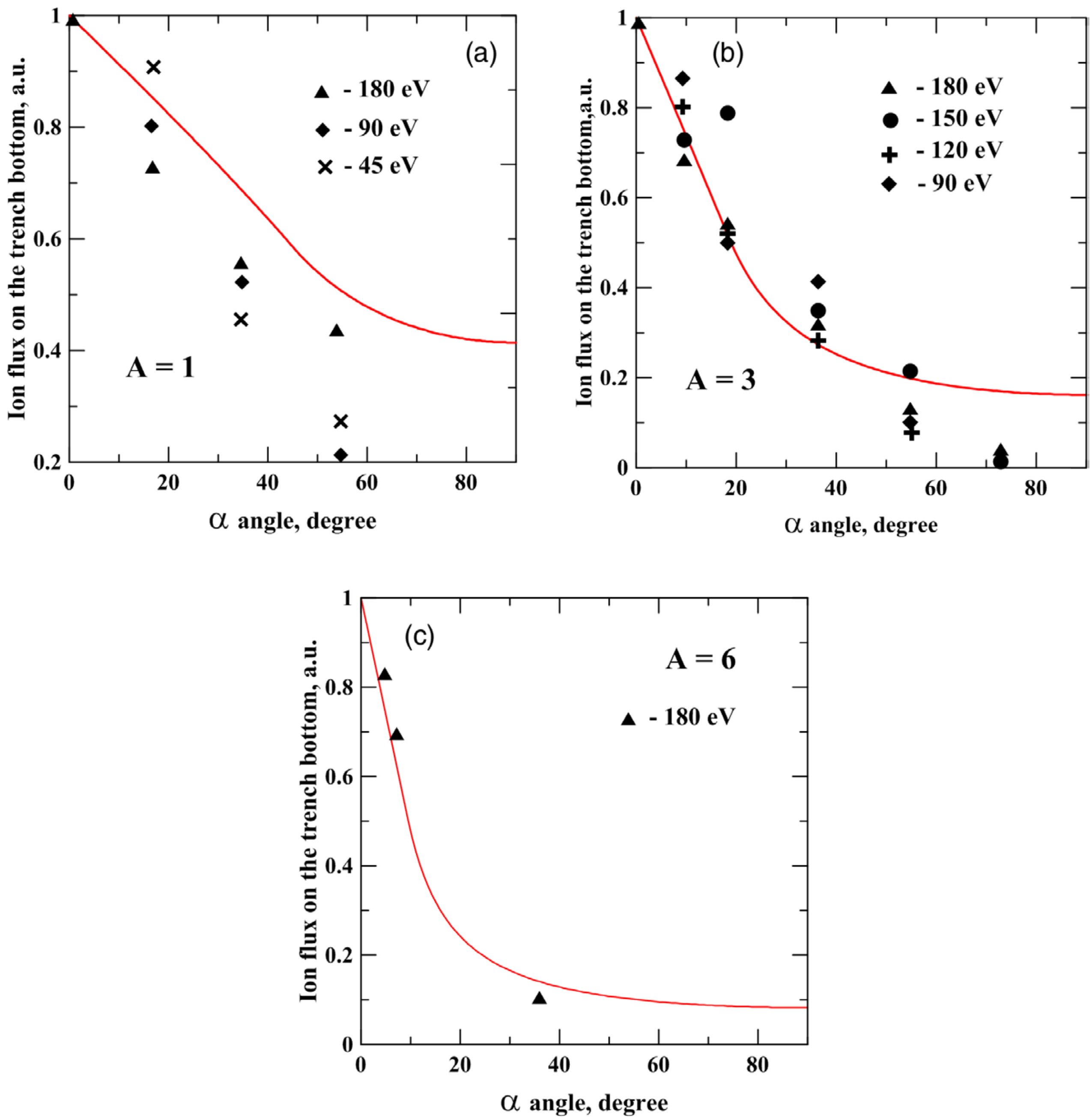

Figure 9. (a) The total ion flux on the trench bottom as a function of the maximal polar angle α of the ion angular distribution function for $A = 1$. The triangles, diamonds, and crosses are the electric potentials on the trench bottom in arbitrary units (a.u.) calculated with Monte Carlo methods. (b) The total ion flux on the trench bottom as a function of the maximal polar angle of the ion angular distribution function for $A = 3$. The triangles, diamonds, and crosses are the electric potentials on the trench bottom in a.u. calculated with Monte Carlo methods. (c) The total ion flux on the trench bottom as a function of the maximal polar angle α of the ion angular distribution function for $A = 6$. The triangles are the electric potentials on the trench bottom in a.u. calculated with Monte Carlo methods.

Let us demonstrate the dependence of the net ion flux on the trench bottom on the maximal angle α can be applied to the estimation of the same dependence of the electric potential. It does not look obvious at first glance because the electric potential also depends on the net number of electrons trapped on the trench bottom. This number of electrons is formed by electron fluxes on the trench bottom, which consist of the electron trajectories curved in the electric field and the electrons generated by the SEE mechanism. In the absence of experimental data we applied a Monte Carlo method on the basis of our physical model considering both the electron trajectory curving and the SEE mechanism [24] to calculate the dependence of the electric potential on the trench bottom on different trench ARs, as well as the ion energy and angular distributions. The ion energies were chosen in the range of 45–180 eV to decrease the presence of the negative potential on the ion trajectories at the trench inlet. The obtained results for a trench width of 12 nm and trench ARs of 1, 3, and 6 are shown in figures 9(a)–(c), respectively. The results of the Monte Carlo modeling shown in figures 9(a)–(c) confirm the found analytic regularities very well. The best agreement between the analytic and numerical results is obtained for

ARs of 3 and 6 when the electron flux on the trench bottom is generated mainly by the SEE mechanism, which dominates the curving of the plasma electron trajectories in an electric field at high ARs. For $A = 1$ the disagreement of the analytic and numerical results is more noticeable. This can probably be explained by the dominance of the curving of the plasma electron trajectories in an electric field over the SEE mechanism for small values of ARs. Thus, further work will be required to consider the effects of electron fluxes on the formation of the electric potential on the trench bottom. Nevertheless, the obtained analytic formulas given by equation (12) could be suggested for the express estimation of the IADF dependence of the electric potential on the trench bottom.

Finally, the advantages of the proposed analytical approach are its simplicity and capability for further extension. It can be applied with a few changes to trenches with conical shapes or extended to three-dimensional (3D) cylindrical geometry. Including electron fluxes of both natures will allow one to calculate the absolute values of the electric potential on the trench bottom. Considering the probability of ion sputtering from the wall surfaces results in the calculation of ion mass transport in the trench and the effects of trench charging on it.

IV. Conclusion

In this paper, ion flux bombarding the trench bottom was calculated analytically for the first time as a function of the ion angular distribution in the range of $\alpha = 0 - \pi/2$ and the trench AR. The analytical dependence of the ion flux on the trench bottom on a trench AR was found, as well as the IADF correlating well with the Monte Carlo numerical calculations of the electric potential on the trench bottom. These Monte Carlo calculations involve both the curving of the charge particle trajectories in an electric field and the SEE mechanism.

The best correlation was found for the maximal angles α, less than 20°, i.e. ones typical for plasma processing technology. This fact allows us to introduce the obtained formula, namely equation (12), for a quick analytic estimation of the electric potential on the trench bottom as a function of the trench AR and the IADF without the necessity of running time-consuming Monte Carlo charging programs. We also expect to apply this formula in Monte Carlo etching codes to consider the impact of an electric field on ionic and electron trajectories in a trench.

In this paper, we also presented the analytical formulas (equations (13)–(17)) of ionic flux distribution over the trench walls and bottom as a function of the AR and the IADF for the first time. We expect the obtained dependences to be helpful for understanding physical processes such as charging and etching for plasma processing technology.

Acknowledgments

A P Palov, Yu A Mankelevich, and T V Rakhimova thank the Russian Science Foundation (RSF) for financial support (Grant № 14-12-01012).

Appendix

First of all let us consider the derivation details of the main equation (12) of this paper. There are three cases and we start from the simplest one when $\theta_{cr} \leqslant \alpha \leqslant \pi/2$. To obtain equation (6) one needs to substitute the integration limits given by equation (5) into equation (3) to take the integral over the available angles:

$$\begin{aligned} F(\alpha, A) &= \frac{N_{\text{ion}}}{2R\sin\alpha}\int_0^R \mathrm{d}r \int_{-\theta_1}^{\theta_2}\cos\theta\,\mathrm{d}\theta \\ &= \frac{N_{\text{ion}}}{2R\sin\alpha}\int_0^R \mathrm{d}r\left\{\sin\left(\tan^{-1}\frac{R+r}{H}\right)+\sin\left(\tan^{-1}\frac{R-r}{H}\right)\right\} \\ &= \frac{N_{\text{ion}}}{2R\sin\alpha}\int_0^R \mathrm{d}r\left\{\frac{R-r}{\sqrt{H^2+(R-r)^2}}+\frac{R+r}{\sqrt{H^2+(R+r)^2}}\right\} \end{aligned} \tag{A.1}$$

The integration of the last line over the initial ion positions on the trench inlet leads us to:

$$\begin{aligned} F(\alpha, A) &= \frac{N_{\text{ion}}}{2R\sin\alpha}\left\{\sqrt{H^2+(R+r)^2}\Big|_0^R - \sqrt{H^2+(R-r)^2}\Big|_0^R\right\} \\ &= \frac{N_{\text{ion}}}{2R\sin\alpha}\left\{\sqrt{H^2+4R^2}-H\right\} \\ &= \frac{N_{\text{ion}}}{\sin\alpha}\left\{\sqrt{A^2+1}-A\right\} \end{aligned} \tag{A.2}$$

where $A = H/2R$ is an AR.

The second case considers the angular range $\theta_c \leqslant \alpha \leqslant \theta_{cr}$. The top angular limit is the same as in our previous calculations, see equation (A.1). The low angular limit, see equation (8) depends on r, thus the integration over r must be split into two parts. As the first step we integrate over angles and over r for the top angular limit:

$$\begin{aligned} F(\alpha, A) &= \frac{N_{\text{ion}}}{2R\sin\alpha}\int_0^R \mathrm{d}r \int_{-\theta_1}^{\theta_2}\cos\theta\,\mathrm{d}\theta \\ &= \frac{N_{\text{ion}}}{2R\sin\alpha}\int_0^R \mathrm{d}r\left\{\sin\left(\tan^{-1}\frac{R-r}{H}\right)+\sin\theta_1\right\} \\ &= \frac{N_{\text{ion}}}{2R\sin\alpha}\left\{-\sqrt{H^2+(R-r)^2}\Big|_0^R + \int_0^R \sin\theta_1\,\mathrm{d}r\right\} \end{aligned} \tag{A.3}$$

The integration of the last line over the initial ion positions on the trench inlet leads us to:

$$\begin{aligned} F(\alpha, A) &= \frac{N_{\text{ion}}}{2R\sin\alpha}\left\{-\sqrt{H^2+(R-r)^2}\Big|_0^R + \int_0^{r*}\sin\left(\tan^{-1}\frac{R+r}{H}\right)\mathrm{d}r \right. \\ &\quad \left. + \int_{r*}^R \sin\alpha\,\mathrm{d}r\right\} \\ &= \frac{N_{\text{ion}}}{2R\sin\alpha}\left\{-\sqrt{H^2+(R-r)^2}\Big|_0^R + \sqrt{H^2+(R+r)^2}\Big|_0^{r*} \right. \\ &\quad \left. + (R-r*)\sin\alpha\right\} \\ &= \frac{N_{\text{ion}}}{2R\sin\alpha}\left\{-H+\sqrt{H^2+(R+r*)^2}+(R-r*)\sin\alpha\right\} \end{aligned} \tag{A.4}$$

Substituting $r^* = H \times \tan(\alpha) - R$ in equation (A.4) one gets equation (9):

$$F(\alpha, A) = \frac{N_{\text{ion}}}{2R\sin\alpha}\left\{(2R - H\tan\alpha)\sin\alpha + \sqrt{H^2(1+\tan^2\alpha)} - H\right\}$$
$$= \frac{N_{\text{ion}}}{2R\sin\alpha}\{2R\sin\alpha - H\sin^2\alpha/\cos\alpha + H/\cos\alpha - H\}$$
$$= N_{\text{ion}}\left\{1 - A\frac{1-\cos\alpha}{\sin\alpha}\right\} \tag{A.5}$$

The third case describes the angular range $0 \leqslant \alpha \leqslant \theta_c$. The low angular limit is simple. The top angular limit, see equation (11) depends on r, thus the integration over r must be split into two parts. As the first step we integrate over angles and over r for the low angular limit:

$$F(\alpha, A) = \frac{N_{\text{ion}}}{2R\sin\alpha}\int_0^R \mathrm{d}r \int_{-\theta_1}^{\theta_2}\cos\theta\,\mathrm{d}\theta$$
$$= \frac{N_{\text{ion}}}{2R\sin\alpha}\int_0^R \mathrm{d}r\{\sin\theta_2 + \sin\alpha\} \tag{A.6}$$
$$= \frac{N_{\text{ion}}}{2R\sin\alpha}\left\{\int_0^R \sin\theta_2\,\mathrm{d}r + R\sin\alpha\right\}$$

The integration of the last line over the initial ion positions on the trench inlet leads one to:

$$F(\alpha, A) = \frac{N_{\text{ion}}}{2R\sin\alpha}\left\{\int_0^{r*}\sin\alpha\,\mathrm{d}r + \int_{r*}^{R}\sin\left(\tan^{-1}\frac{R-r}{H}\right)\mathrm{d}r + R\sin\alpha\right\}$$
$$= \frac{N_{\text{ion}}}{2R\sin\alpha}\left\{(R - H\tan\alpha)\sin\alpha - \sqrt{H^2 + (R-r)^2}\Big|_{r*}^{R} + R\sin\alpha\right\}$$
$$= \frac{N_{\text{ion}}}{2R\sin\alpha}\{(2R - H\tan\alpha)\sin\alpha - H + H/\cos\alpha\}$$
$$= N_{\text{ion}}\left\{1 - A\frac{1-\cos\alpha}{\sin\alpha}\right\} \tag{A.7}$$

We see the final results for the second and third cases are identical. So, after merging equations (A.2), (A.5) and (A.7) we obtain the main formula equation (12) of this paper:

$$F_{\text{ion}}(\alpha, A) = \begin{cases} N_{\text{ion}}\left\{1 - A \times \dfrac{1-\cos\alpha}{\sin\alpha}\right\}, & 0 \leqslant \alpha \leqslant \theta_{\text{cr}} \\ \dfrac{N_{\text{ion}}}{\sin\alpha}\left\{\sqrt{1+A^2} - A\right\}, & \theta_{\text{cr}} \leqslant \alpha \leqslant \pi/2 \end{cases} \tag{A.8}$$

The total ion fluxes on the trench walls given by equation (14) can be obtained from equation (13), written for convenience for the left wall as:

$$F_{\text{ion}}(\alpha, R, H) = \frac{N_{\text{ion}}}{4R\sin\alpha}\int_0^{r*}\mathrm{d}r\int_{-\alpha}^{-\theta_2}\cos\,\mathrm{d}\theta$$
$$= \frac{N_{\text{ion}}}{4R\sin\alpha}\int_0^{r*}\mathrm{d}r\left\{-\frac{r}{\sqrt{H^2+r^2}} + \sin\alpha\right\}$$
$$= \frac{N_{\text{ion}}}{4R\sin\alpha}\left\{r*\sin\alpha - \sqrt{H^2+r^2}\Big|_0^{r*}\right\}$$
$$= \frac{N_{\text{ion}}}{4R\sin\alpha}\left\{r*\sin\alpha - \sqrt{H^2+r^{*2}} + H\right\} \tag{A.9}$$

where $\theta_2 = \tan^{-1}(r/H)$. Now we need to consider two cases. The first one for angles in the range of $0 \leqslant \alpha \leqslant \theta_{\text{cr}}$ leads to the maximal value $r^* = H \times \tan(\alpha)$ and the ion flux coming from the trench inlet on one wall of height H:

$$F_{\text{ion}}(\alpha, R, H) = \frac{N_{\text{ion}}}{4R\sin\alpha}\{H\sin^2\alpha/\cos\alpha - H/\cos\alpha + H\}$$
$$= \frac{N_{\text{ion}}}{2}\frac{H}{2R}\frac{1-\cos\alpha}{\sin\alpha} \tag{A.10}$$

The factor 1/2 considers one wall only in the final line. The second case for angles in the range of $\theta_{\text{cr}} \leqslant \alpha \leqslant \pi/2$ leads to the maximal value $r^* = 2R$ and the ion flux coming to a wall of height H in accordance with equation (A.9) becomes:

$$F_{\text{ion}}(\alpha, R, H) = \frac{N_{\text{ion}}}{4R\sin\alpha}\left\{2R\sin\alpha - \sqrt{H^2+4R^2} + H\right\}$$
$$= \frac{N_{\text{ion}}}{2\sin\alpha}\left\{\sin\alpha - \sqrt{1+\left(\frac{H}{2R}\right)^2} + \frac{H}{2R}\right\} \tag{A.11}$$

If we want to get an ion flux on one cell on the wall we need to take two total fluxes; one covers the wall length from the beginning of the trench at h = 0 until the height $h = x$, and the other flux covers the length from $H = 0$ until $H = x + \mathrm{d}x$, where dx is the size of a cell. At the next step we need to subtract the first flux from the last one. To make it for the whole wall one needs to digitize it. Let us introduce instead of H its discrete equivalents $H_i = i \times h$ and $H_{i+1} = (i+1) \times h$, where h is a grid spacing in the trench height direction, and then the ion flux on the ith cell of the grid $\Delta F_i = F_{\text{ion},\ i+1}(\alpha,\ A_{i+1}) - F_{\text{ion},\ i}(\alpha,\ A_i)$ with $A_i = H_i/2R$ can be written in accordance with equations (A.10) and (A.11):

$$\Delta F_i(\alpha, R, h) = \begin{cases} \dfrac{N_{\text{ion}}}{2}\dfrac{h}{2R}\dfrac{1-\cos\alpha}{\sin\alpha}, & 0 \leqslant \alpha \leqslant \theta_{\text{cr}} \\ \dfrac{N_{\text{ion}}}{2\sin\alpha}\left\{\dfrac{h}{2R} + \sqrt{1+\left[\dfrac{ih}{2R}\right]^2} - \sqrt{1+\left[\dfrac{(i+1)h}{2R}\right]^2}\right\}, & \theta_{\text{cr}} \leqslant \alpha \leqslant \dfrac{\pi}{2} \end{cases} \tag{A.12}$$

which is exactly the same as equation (14).

Let us consider how equation (17) for the ion distribution over the trench bottom can be obtained from equation (15). First, we need to integrate equation (15) over angles and substitute the angular integration limits from equation (16):

$$\Delta F_j(\alpha, A) = \frac{N_{\text{ion}}}{2\sin\alpha}\int_{r_{\min}}^{r_{\max}}\mathrm{d}r\int_{-\theta_1}^{-\theta_2}\cos\theta\,\mathrm{d}\theta$$
$$= \frac{N_{\text{ion}}}{2\sin\alpha}\int_{r_{\min}}^{r_{\max}}\mathrm{d}r\{\sin(-\theta_2) - \sin(-\theta_1)\}$$
$$= \frac{N_{\text{ion}}}{2\sin\alpha}\int_{r_{\min}}^{r_{\max}}\mathrm{d}r\left\{-\frac{x_2}{\sqrt{1+x_2^2}} + \frac{x_1}{\sqrt{1+x_1^2}}\right\} \tag{A.13}$$

where $x_1 = (r - r_{j-1})/A$ and $x_2 = (r - r_j)/A$, the $r_{j-1} = (j-1)\Delta r/2R$ and $r_j = j\Delta r/2R$ are the positions of the $(j-1)$th and jth cells on the trench bottom, respectively, $r = x/2R$ and x is a position of the initial ion flux on the trench inlet. Second, we have to take the integral over r substituting the above-mentioned x_2 and x_1 and the values of $r_{\max}$ and $r_{\min}$ taken from equation (15):

$$\Delta F_j(\alpha, A) = \frac{N_{\mathrm{ion}}}{2\sin\alpha} A \left\{ \sqrt{1+x_1^2}\,\Big|_{r_{\min}}^{r_{\max}} - \sqrt{1+x_2^2}\,\Big|_{r_{\min}}^{r_{\max}} \right\}$$
$$= \frac{N_{\mathrm{ion}}}{2\sin\alpha} \left\{ \sqrt{A^2+(r-r_{j-1})^2}\,\Big|_{r_{\min}}^{r_{\max}} - \sqrt{A^2+(r-r_j)^2}\,\Big|_{r_{\min}}^{r_{\max}} \right\}$$
$$= \frac{N_{\mathrm{ion}}}{2\sin\alpha} \left\{ \begin{array}{l} \sqrt{A^2+(r_{\max}-r_{j-1})^2} - \sqrt{A^2+(r_{\min}-r_{j-1})^2} \\ +\sqrt{A^2+(r_{\min}-r_j)^2} - \sqrt{A^2+(r_{\max}-r_j)^2} \end{array} \right\} \quad \text{(A.14)}$$

which leads exactly to equation (17).

References

[1] Donnelly V M and Kornblit A 2013 *J. Vac. Sci. Technol.* **A31** 050825
[2] Yagisawa T, Maeshige K, Shimada T and Makabe T 2004 *IEEE Trans. Plasma Sci.* **32** 90
[3] Hashimoto K 1993 *Japan. J. Appl. Phys.* 1 **32** 6109
[4] Hashimoto K 1994 *Japan. J. Appl. Phys.* 1 **33** 6013
[5] Yoshida Y and Watanabe T 1983 *Proc. 5th Symp. Dry Process (Tokyo)* p 4
[6] Baklanov M R, de Marneffe J-F, Shamiryan D, Urbanowicz A M, Shi H, Rakhimova T V, Huang H and Ho P S 2013 *J. Appl. Phys.* **113** 041101
[7] Bogaerts A, Bultinck E, Eckert M, Georgieva V, Mao M, Neyts E and Schwaederle L 2009 *Plasma Process. Polym.* **6** 295
[8] Wijesundara M B J, Hanley L, Ni B and Sinott S B 2000 *Proc. Natl Acad. Sci. USA* **97** 23
[9] Zhang D and Kushner M 2000 *J. Appl. Phys.* **87** 1060
[10] Economou D 2000 *Thin Solid Films* **365** 348
[11] Hitchon W 1999 *Plasma Processes for Semiconductor Fabrication* (Cambridge: Cambridge University Press)
[12] Arnold J C and Sawin H H 1991 *J. Appl. Phys.* **70** 5314
[13] Kinoshita T, Hane M and McVittie J P 1996 *J. Vac. Sci. Technol.* B **14** 560
[14] Hwang G S and Giapis K P 1997 *Appl. Phys. Lett.* **71** 1945
[15] Kortshagen U 1998 *J. Vac. Sci. Technol.* A **16** 300
[16] Converse M 1999 *IEEE Trans. Plasma Sci.* **27** 1441
[17] Matsui J, Maeshige K and Makabe T 2001 *J. Phys. D: Appl. Phys.* **34** 2950
[18] Radjenovic B, Radmilovic-Radjenovic M and Petrovich Z Lj 2007 *Mater. Sci. Forum.* **555** 53
[19] Zhang Y, Kushner M, Moore N, Pribyl P and Gekelman W 2013 *J. Vac. Sci. Technol.* A **31** 061311
[20] Zhang S, Dai Z and Wang Y 2012 *Plasma Sci. Technol.* **14** 958
[21] Radmilovic-Radjenovic M, Radjenovic B and Savic M 2011 *Int. J. Numer. Model.* **24** 535
[22] Liu J, Huppert G L and Sawin H H 1990 *J. Appl. Phys.* **68** 3916
[23] Woodworth J R, Miller P A, Shul R J, Abraham I C, Aragon B P, Hamilton T W, Willison C G, Kim D and Economou D J 2003 *J. Vac. Sci. Technol.* A **21** 147
[24] Palov A P, Mankelevich Yu A, Rakhimova T V and Shamiryan D 2010 *J. Phys. D: Appl. Phys.* **43** 075203
[25] Palov A P, Mankelevich Yu A, Rakhimova T V and Shamiryan D 2010 *Plasma Phys. Rep.* **36** 891